TWENTIETH EUROPEAN ROTORCRAFT FORUM

Paper No. 11

Prediction - and its Validation - of the Acoustics of Multiblade Rotors in Forward Flight Utilising Pressure Data from a 3-D Free Wake Unsteady Panel Method

Jian P. YIN*), Syed R. AHMED
DLR, Institute of Design Aerodynamics
Lilienthalplatz 7, 38108 Braunschweig
Germany

October 4 - 7, 1994

Amsterdam, The Netherlands

*) Guest Scientist, Nanjing University of Aeronautics & Astronautics, Nanjing, People's Republic of China

Prediction - and its Validation - of the Acoustics of Multiblade Rotors in Forward Flight Utilising Pressure Data from a 3-D Free Wake Unsteady Panel Method

Jian P. YIN*), Syed R. AHMED
DLR, Institute of Design Aerodynamics
Lilienthalplatz 7, 38108 Braunschweig
Germany

*) Guest Scientist, Nanjing University of Aeronautics & Astronautics, Nanjing, People's Republic of China

ABSTRACT

A newly developed high resolution 3-D Panel method to predict the unsteady aerodynamics of multiblade helicopter rotors has been used to generate the input data for an also new Acoustics code based on Farassat's Formulation 1A of the FWH-equation.

The combination of this aerodynamics/aeroacoustics codes is used to predict the acoustics of multiblade rotors in hover and forward flight. Of special interest are cases of low speed descent where severe BVI is known to occur. The use of panel method excludes the treatment of shocks in the rotor flow field. No restrictions are placed on the blade profile, planform or other geometry characteristics as well as blade motions.

The acoustic pressure-time history, mid-frequency sound pressure levels and other predictions are validated with flight test and wind tunnel data for two and four blade rotors in hover and forward descent flight modes. Some comparisons with the predictions of the well known WOPWOP code have also been performed.

Good to fair agreement of the predictions with the flight test and wind tunnel results has been obtained.

INTRODUCTION

Helicopters have proven to be a very versatile means of transportation and fulfill a unique role in civil and military aviation. As the helicopter became more mature and its use expanded, helicopter generated noise - and rotor noise in particular - has become an increasingly important problem for the helicopter designer.

Both the FAA and ICAO noise certification requirements for new helicopters have made helicopter noise to receive serious attention early in the design process instead of as a problem during production and at the same time elevated the importance of the noise to nearly the same level as performance, safety and reliability etc.

In both civil and military applications the helicopter passes through flight regimes (low speed forward descent flight as an example) in which vortices in the rotor wake interact with the blades, causing sudden changes in blade loading which contributes to one of the characteristic noises from the helicopter - the so called "blade slap", or impulsive noise. Blade slap or impulsive noise is one of the subjectively more annoying noises and also contributes significantly to the detectability of a helicopter. Therefore, future applications of helicopters may be limited due to community environment and noise concerns and also military detectability considerations. Improving the performance of the helicopter while reducing the radiated noise is a real challenge for the helicopter designer.

In order to compute the rotor noise, it is necessary to have a detailed knowledge of the loads or surface pressures acting upon the blades. There are two ways to obtain the blade loading: through theoretical prediction or by experimental measurement. Once these aerodynamic data are available, one of the several approaches to compute the radiated acoustic pressure and spectra may be taken [1].

Due to the simultaneous interaction of a number of aerodynamic phenomena, the flow field around a helicopter rotor is extremely complex and accounts for most of the aeroacoustic differences between a helicopter rotor and an airplane propeller. The asymmetry of the velocity distribution which the helicopter rotor experiences is a result of the superposition of the rotational motion and the forward flight speed. The flow field is three-dimensional, highly unsteady and may contain transonic flow regions or be greatly influenced by viscosity.

The unsteadiness of the flow field under forward flight condition can be related to two main sources: the first one is introduced by the cyclic variation of the free stream velocity relative to the rotor blades, and the cyclic variation of the blade pitch, flapping and lead-lag motion; the second one is caused by rotor blade interaction with its own distorted wake and wakes of preceding blades. The mutual interference between the rotor blades and their wake is very important in all types of helicopter motion,

Presented at the 20th European Rotorcraft Forum,
Amsterdam, The Netherlands, October 4 - 7, 1994

especially in descending flight in which the wake moves up through the rotor disc.

Compressibility effects become important on the advancing blade once the flow becomes transonic, especially in high speed forward flight and near the blade tip. Also the increased pitch on the retreating blade may cause dynamic stall over a considerable portion of the rotor disc. In addition, the flow reversal/flow separation region at the blade root on the retreating side becomes large with increasing speed.

In a full simulation of such complex phenomena these important unsteady viscous effects must also be accounted for. As a result of these diverse aerodynamic phenomena, the computation of the flow field around a multiblade helicopter rotor considering all the above effects represents an extremely difficult task and is almost impossible to achieve at the present time. However, if certain important aspects are singled out, such as the blade vortex interaction and unsteadiness of the flow field, neglecting the viscous effects, the problem is amenable to analysis and solution.

Inviscid aerodynamics is the primary field for most of the advanced methods which are currently used for rotors. Because the interference effect between the blade and its shed wake is an important aspect of flow around a rotor blade, it needs to be carefully simulated. The helical geometry of the rotor wake implies that its detailed spatial configuration is important even at scales on the order of the rotor size. In order to obtain a more accurate prediction of the "aerodynamics" around the rotor blades, a wake model which can represent its distortion and roll-up must be incorporated in the code.

Presently there are two frequently used techniques to predict the wake geometry:
one is an Euler-Lagrangian approach, in which a full potential method simulates the rotor blades and the shed vorticity is modelled by "markers" convected with the flow [2]. The compressible flow around the blade and a non-dissipative convection of the wake is calculated, but the disadvantage of this method is the need for a priori knowledge of the wake geometry. The second approach is the solution of Navier-Stokes equations, which can capture more of the physical behavior implicitly contained in the equations and describe the generation, transport and structure of the wake vorticity [3]. The above-mentioned field methods need presently much bigger computing effort in order to adequately resolve the vortices in the wake.

Due to these limitations these methods are not well suited for parametric studies. The need for a simple and relatively inexpensive prediction method for the rotor aerodynamics, not restricted to a particular flight condition is thus imperative.

With the consideration that an important design goal of modern rotors is to reduce the sonic region near the blade tip and that over a significant part of helicopter flight envelope the flow field around the major part of the rotor blades remains shock-free, the flow field can be considered basically as incompressible.

The importance of including unsteady effects in rotor calculation has been emphasized in the review paper of Byham and Beddoes [4]. The unsteady incompressible flow about a two-dimensional airfoil of arbitrary shape executing arbitrary time-dependent motion was developed by Giesing [5] and is based on a steady panel method. In this method the free wake is generated step by step as the calculation proceeds in time. This method was extended by Summa [6] to calculate the problem of potential flow about more complex configurations. Based on these concepts an unsteady 3-D panel method has been developed recently by S. R. Ahmed [7] to compute the subsonic aerodynamics of *finite thickness* multiblade rotors and extended in [8] to include realistic rotor blade pitch, flapping and lead-lag motions. Radiated noise from rotors, especially during descent, is known to be significantly influenced by blade airfoil characteristics. So the simulation of the real blade geometry and its motions means a more precise modeling of the rotor flow. In the present paper, the surface pressure of the rotor blade computed by the unsteady 3-D panel method mentioned above is used to determine the loading noise in the acoustic code.

Over the past years, a substantial progress has been made in the science and technology of the helicopter rotor noise research. The most recent activity is the EC Helinoise programme which brings together researchers throughout Europe from manufacturers, universities and research institutes in a combined theoretical and experimental programme. A detailed summary of current status on the theoretical work was given in ref. [9].

A new numerical aeroacoustics code, named HRNPC has been developed under a cooperation project between DLR and CAE (Chinese Aeronautics Establishment). The code is based on the well-known Farassat time domain Formulation 1a for the determination of the thickness and loading noise. The code can calculate loading noise, either from theoretical or experimental load data.

The purpose of the present paper is two-fold: firstly, measured model-rotor blade pressure data recently obtained in DNW [10] is used as input for non-compact loading noise prediction and compared with direct noise measurement results. Secondly, theoretical blade load data from 3-D unsteady panel method has been used to predict the noise characteristics of two and four blade rotors in hover and forward descent flight and validate it with results of other theoretical work and experiments.

DESCRIPTION OF THE METHOD

The Aerodynamics Code

Panel methods are numerical schemes for the solution of potential flow problems and are capable of treating flows about complex three-dimensional configurations. In the specific case of unsteady rotor flows the boundary condition of flow tangency on the blade surface at *every instant in time* need to be imposed on the solution. A detailed description of the 3-D unsteady panel method used for the results of this paper is given in [7, 8].

The model of the lifting rotor blade used here (at any time instant) consists of (Fig. 1):

- a source/sink distribution of unknown strength over the blade surface
- a doublet distribution of unknown strength (but of prescribed chordwise variation) over the mean surface inside the blade
- a zero-thickness elongation (2% of local blade chord) of the blade trailing edge (Kutta panel) carrying a doublet distribution of unknown strength.

The numerical procedure consists of dividing the blade, the internal and the wake surfaces into *finite surface* elements (see Fig. 1). The unknown source/sink or doublet strength on each surface element is assumed to be *constant.* Additionally, the equivalence of constant strength doublet panels and vortex rings ([11]) is used to replace the doublet panels by vortex rings of same strength placed on the perimeter of the doublet panels. Induced velocities for a quadrilateral doublet panel are then, for example, calculated from the four vortex line filaments at the panel edge using Biot-Savart law.

Imposing the flow tangency condition at a number of discrete points P on the blade and Kutta panel surface leads to a system of *linear* algebraic equations whose iterative solution gives the strength of the singularities for each of the generic points P at a time instant t. As mentioned earlier, the variation of circulation strength on the profile mean line is *prescribed.* The circulation strength of the Kutta panel is set equal to that at the trailing edge. Once the Kutta panel strength is known the relative strengths of all vortex panels on the mean surface are known.

The calculation proceeds in the following manner:

At time $t = 0$, the rotor is impulsively started from rest from a given azimuthal position. At this instant, there is no wake. With the solution of the system of equations, the strength of the singularities on the blade surface and circulation strength of vortex rings on Kutta panels is known. Using these singularities, the induced velocities at the downstream corner points (e.g. A and B in Fig. 1) of Kutta panels are evaluated. A straight vortex element is released now from the trailing edge of each Kutta panel. The ends of this vortex element are moved with the calculated induced velocities plus the velocity components due to translation, rotation and other motions of the blade over a time interval Δt. This vortex filament, together with the so created downstream segments and the Kutta panel trailing edge, comprises a quadrilateral ring vortex (A, B, C, D in Fig. 1). Its strength is equal to that of the Kutta panel from which it was released. This row of vortex panels released from the Kutta panels is the increment of the blade wake after Δt. The distortion of the "wake" is effected by the differing velocities with which the end points of the released vortex filaments move. Once a row of vortex panels has been assigned a certain spanwise variation of circulation, the circulation distribution for this particular row of panels remains constant as the wake panels move and distort in space. This fulfills the dynamical boundary condition of zero pressure difference across the wake [9]. For the next time step, the system of equations is solved anew, taking into consideration now the induction of the first row of vortex panels at all collocation points. This process is repeated until the blade aerodynamics converge to a desired behavior.

The Aeroacoustics Code

Governing Equations

The formulation used in the HRNPC aeroacoustics code of this paper is the Formulation 1a of Farassat [12], which is an integral of the Ffowcs Williams-Hawkings (FWH) equation with thickness and loading source terms only. Quadrupole noise is believed to be small compared to thickness and loading noise in the shock-free rotor flow examples dealt with here. The computations are performed in the time domain resulting in an acoustic time series which is Fourier analyzed to obtain the acoustic spectrum.

The posed problem is mathematically described by the following integral equation governing the noise radiation from a moving source, referred to as Farassat's Formulation 1a:

$$4\pi P'_T\ (\vec{x}, t) = \int_{f=0} \left[\frac{\rho_0 \dot{V}_n}{r(1-M_r)^2}\right]_{ret} dS + \int_{f=0} \left[\frac{\rho_0 V_n\left(r\dot{M}_i\hat{r}_i + c_0 M_r - c_0 M^2\right)}{r^2(1-M_r)^3}\right]_{ret} dS \qquad [1]$$

$$4\pi P'_L\ (\vec{x}, t) = \frac{1}{c_0}\int_{f=0}\left[\frac{\dot{l}_i\hat{r}_i}{r(1-M_r)^2}\right]_{ret} dS + \int_{f=0}\left[\frac{l_r - l_i M_i}{r^2(1-M_r)^2}\right]_{ret} dS + \frac{1}{c_0}\int_{f=0}\left[\frac{l_r\left(r\dot{M}_i\hat{r}_i + c_0 M_r - c_0 M^2\right)}{r^2(1-M_r)^3}\right]_{ret} dS \qquad [2]$$

Here P'_T and P'_L denote the acoustic pressure due to thickness and loading noise respectively. The sum of P'_T and P'_L is the total acoustic pressure. The integration is carried out over the area element dS on the surface $f = 0$ which represents the blade surface. The subscript 'ret' denotes that the integrand is evaluated at a retarded time $\tau = t - r/c$, where t is the observer time and $r = |\vec{x} - \vec{y}|$. Here vector $\vec{y}$ and $\vec{x}$ are the source and observer positions respectively. Hereby

$$M_r = \frac{\partial\vec{y}}{c_0\partial\tau}\cdot\frac{\vec{r}}{|\vec{r}|} = (V_i\hat{r}_i)/c_0$$

is the Mach number in the radiation direction $\vec{r}$ for a point $\vec{y}$ lying on the rotor blade. $l_r = l_i\hat{r}_i$ is the force acting on the fluid per unit area in the radiation direction. The quantity l_i is equal to $P_{ij}\hat{n}_j$, where P_{ij} is the Reynold's stress tensor that includes the surface pressure and viscous stresses and $\hat{n}_j$ is the unit outward normal vector to the surface of the rotor blade $f = 0$. The information required for the thickness noise is purely geometrical in nature and is obtained simply from the definition of blade thickness and motion. ρ_0 and c_0 are the density and speed of sound of the undisturbed medium, respectively.

The dots on $\dot{M}_i$, $\dot{l}_i$ and $\dot{V}_n$ describe the rate of variation of these quantities with respect to the source time, where $\dot{M}_i = \dot{V}_i/c$ and $\dot{V}_n$ are local and local normal acceleration of the blade respectively. Since in potential flow $l_i = Pn_i$ (with surface pressure P defined as $P_a - P_\infty$, and P_a as the absolute surface pressure and P_∞ is the ambient pressure), $\dot{l}_i = \dot{P}n_i + P\dot{n}_i$. Therefore $\dot{l}_i \neq 0$ even if l_i is a constant. In the case of potential flow, Farassat's Formulation 1a can be rewritten as follows:

$$4\pi P'_T\ (\vec{x}, t) = \int_{f=0}\left[\rho_0 c_0^2\frac{\dot{M}_n}{c_0 r(1-M_r)^2}\right]_{ret} dS + \int_{f=0}\left[\rho_0 c_0^2\frac{M_n\left(r\dot{M}_i\hat{r}_i + c_0 M_r - c_0 M^2\right)}{c_0 r^2(1-M_r)^3}\right]_{ret} dS \qquad [3]$$

$$4\pi P'_L\ (\vec{x}, t) = \int_{f=0}\left[\dot{P}\frac{\hat{n}_i\hat{r}_i}{c_0 r(1-M_r)^2}\right]_{ret} dS + \int_{f=0} P\left[\frac{\dot{\hat{n}}_i\hat{r}_i}{c_0 r(1-M_r)^2} + \frac{\hat{n}_i\hat{r}_i - \hat{n}_i M_i}{r^2(1-M_r)^2} + \frac{\hat{n}_i\hat{r}_i\left(r\dot{M}_i\hat{r}_i + c_0 M_r - c_0 M^2\right)}{c_0 r^2(1-M_r)^3}\right]_{ret} dS \qquad [4]$$

where M is the local Mach number.

Since there are no restrictions placed on the *blade motion* and *geometry*, eqs. (3) and (4) are valid for arbitrary blade motion and geometry.

Numerical Implementation

The rotor is described in a Cartesian blade-fixed frame of reference. The origin of the reference frame is at the intersection of rotor axis η_3 and the blade pitch change axis η_1. The third axis η_2 is taken normal to η_1, η_3-plane in such a way that the η-reference frame is right-handed.

The actual acoustic calculations are carried out in a ground-fixed reference frame in which the observer position is fixed. The coordinate transformations between blade-fixed frame of reference $\vec{\eta}$ and ground-fixed frame of reference $\vec{Y}$ used in the present code are expressed by the following transformation matrix

$$\begin{bmatrix} Y_1 \\ Y_2 \\ Y_3 \end{bmatrix} = \begin{bmatrix} V_x\tau \\ V_y\tau \\ V_z\tau \end{bmatrix} + \begin{bmatrix} \cos\alpha & 0 & -\sin\alpha \\ 0 & 1 & 0 \\ \sin\alpha & 0 & \cos\alpha \end{bmatrix}\begin{bmatrix} -\cos\Psi & \sin\Psi & 0 \\ -\sin\Psi & -\cos\Psi & 0 \\ 0 & 0 & 1 \end{bmatrix}$$
$$\begin{bmatrix} \cos\beta & 0 & -\sin\beta \\ 0 & 1 & 0 \\ \sin\beta & 0 & \cos\beta \end{bmatrix}\begin{bmatrix} \cos\zeta & \sin\zeta & 0 \\ -\sin\zeta & \cos\zeta & 0 \\ 0 & 0 & 1 \end{bmatrix} \qquad [5]$$
$$\begin{bmatrix} 1 & 0 & 0 \\ 0 & \cos\Theta & -\sin\Theta \\ 0 & \sin\Theta & \cos\Theta \end{bmatrix}\begin{bmatrix} \eta_1 \\ \eta_2 \\ \eta_3 \end{bmatrix} + \begin{bmatrix} \cos\alpha & 0 & -\sin\alpha \\ 0 & 1 & 0 \\ \sin\alpha & 0 & \cos\alpha \end{bmatrix}$$
$$\begin{bmatrix} -\cos\Psi & \sin\Psi & 0 \\ -\sin\Psi & -\cos\Psi & 0 \\ 0 & 0 & 1 \end{bmatrix}\begin{bmatrix} \cos\beta & 0 & -\sin\beta \\ 0 & 1 & 0 \\ \sin\beta & 0 & \cos\beta \end{bmatrix}\begin{bmatrix} e \\ 0 \\ 0 \end{bmatrix}$$

where

$$\vec{\eta} = \begin{bmatrix} \eta_1 \\ \eta_2 \\ \eta_3 \end{bmatrix} = \begin{bmatrix} Y \\ -X \\ Z \end{bmatrix}$$

is a position vector of a point in the blade-fixed frame and

$$\vec{Y} = \begin{bmatrix} Y_1 \\ Y_2 \\ Y_3 \end{bmatrix}$$

is the position vector of the same point in the ground-fixed frame. A series of four intermediate reference frames has been used to relate the quantities in the $\vec{\eta}$ and $\vec{Y}$ reference frames. These are necessary to include the helicopter *forward motion, blade rotation, flapping, pitching* and *lead-lag motions* as well as the *rotor shaft tilt*. In eq. (5), (V_x, V_y, V_z) are components of the helicopter velocity in Y_1, Y_2, and Y_3 direction, α is the angle between the rotor shaft and the vertical axis, Ψ is the blade azimuth angle, β, ζ and Θ are the blade flapping, blade lead-lag and the blade pitching angle respectively, and e is the lag hinge offset.

The noise calculation in the HRNPC is performed by dividing the rotor blade surface into a number of panels. This discretisation of the blade surface is different from the discretisation used for the aerodynamic code. To capture the BVI phenomena more accurately, the area between 0% and 5% of blade chord and between 85% and 100% of blade span have a finer mesh. A Gauss-Legendre integration is used to determine the panel collocation points on the blade. A comparison of the aerodynamic and aeroacoustic blade surface discretisation of the AH1/OLS rotor is shown in Fig. 2. A numerical integration is carried out assuming the value of the integrand (e.g. sound pressure) at the panel collocation point as remaining constant over the entire panel area. Sound pressure at an observer position is the summed contribution from all the panels at a considered time instant.

Normally, the integration over the curved blade surface can be transformed into integration in a plane and this then further divided into finite integrations in the spanwise η_1 and chordwise η_2 directions. The relationship of this transformation is $dS = N d\eta_1 \, d\eta_2$ where N is the Jacobian of the transformation. Near the leading edge, the curved surface dS tends to be vertical to $d\eta_2$ and the value of the Jacobian tends to infinity. In order to avoid this numerical problem, the airfoil contour length l, starting from the leading edge has been used instead of η_2.

The acoustics computation is performed as follows: Firstly, the source time τ is calculated for a specified observer time t and blade coordinates (η_1, η_2, η_3) to solve the retarded time equation iteratively. Then the azimuth angle Ψ at the retarded time is computed. Now the corresponding blade surface pressure for the specified set of parameters (η_1, η_2, η_3 and Ψ) can be evaluated.

The computed blade pressure time history may not be smooth. To calculate its derivatives, a cubic spline interpolation is used. Curve smoothing is not used because the time derivative contributes a major part to the sound pressure especially in BVI case and even small errors will significantly affect the results. Curve smoothing may also erase important features of the noise signature and spread the BVI pulse over too much area.

The use of a finer mesh for the acoustics calculation than in the aerodynamic code implies that blade pressure values at the 'extra' collocation points of the acoustics mesh have to be obtained through suitable inter- or extrapolation of the aerodynamic code results. This process was guided by the theoretical and experimental experience detailed in [13].

Several strategies were applied in the acoustics code to reduce the CPU time. Firstly, the pressure signature of only one blade is calculated. The signature for the other blades is calculated by shifting this signature to the location of other blades. Further, the retarded time from the last calculation is used as the initial guess for the next calculation to decrease the number of iterations necessary in the calculation of the retarded time.

Validation of the Acoustics Code Predictions

Two Blade UH-1H Rotor in Hover and Forward Flight

As a preliminary validation exercise the aerodynamics of the standard version of the UH-1H 1/4 scale model rotor system, tested in the Langley 4 m x 7 m tunnel [14], were compared by the 3-D unsteady panel method Code (UPMC) and the blade surface pressure used as input for the Acoustics Code HRNPC. The results are validated against experimental data from [14] and theoretical results obtained by the acoustics code WOPWOP described in [12].

The UH-1H two blade rotor investigated has rectangular planform blades with a linear twist distribution and NACA 0012 airfoil sections throughout. The hover case corresponds to the example no. 3 and the forward flight to the example no. 1 cited in [12]. In both examples, the tip Mach number is high to warrant consideration of compressibility effects - namely $Ma_{tip} = 0.73$ in hover and $Ma_{tip} = 0.88$ in forward flight. In the UPMC the compressibility effects are approximately accounted for by an appropriate form of the Goethert rule. However, in the present calculations this correction has not been performed.

Figs. 3a, b illustrate the acoustic pressure-time history for an observer in the tip-path plane during *hover* for one period (half rotor revolution). In Fig. 3a, the present code results for thickness-, loading- and overall noise are shown while in Fig. 3b the corresponding results obtained with the WOPWOP acoustics code are plotted. It is to be noted that the blade loads for our results were calculated with the UPMC run at azimuth steps of 22.5° whereas the aerodynamic input to the WOPWOP code was obtained using a functional relationship between section lift-, thrust- and drag coefficients (see [12], page 59).

In this Figure, the waveform character is dominated by a large negative pressure pulse preceded by a smaller amplitude positive pressure pulse. The breakdown of the overall noise into thickness and loading noise indicates that the large negative pressure peak is created by the displacement effect of the rotating blade on the surrounding air which is counteracted at the same azimuth position by a wider and weaker positive pressure pulse generated by the pressure distribution on the blade surface. The comparison of HRNPC and WOPWOP code results shows a phase shift of approximately 0.025 rotor revolution for the overall and loading noise peaks but the main difference is obviously the different variation of the loading noise which is predicted higher (less negative) on the advancing side and lower (more negative) on the retreating side by the UPMC/HRNPC combination. Essentially these differences can be attributed to the different approaches taken to generate the aerodynamic input for the HRNPC and WOPWOP codes.

Sound pressure level results for the UH-1H rotor in *hover* are compared in Fig. 4 with the corresponding results of WOPWOP code. Also here, as mentioned above, the main difference between the present and WOPWOP predictions concerns the loading noise content of the overall noise. A slight influence of the loading noise on the overall signature is indicated in the present results whereas the WOPWOP prediction shows an effect only till about 6th harmonic.

Similar trends are observed for the UH-1H rotor in forward flight from Figs. 5 and 6. Again the observer position is in the tip path plane, upstream and approximately 33° inclined to the wind tunnel centerline. This corresponds to the position of microphone number 4 in [14].

A direct comparison of the present code results with experimental results from [14] for the 1/4 scale UH-1H rotor model is shown in Fig. 7. The predicted acoustic pressure-time history and sound pressure level for the forward flight situation (for microphone number 4) are in good agreement with the wind tunnel data.

Two Blade AH1/OLS Rotor in Forward Descent Flight

The descent is a particularly interesting flight condition from an acoustics point of view since strong Blade Vortex Interaction (BVI) noise is generated during this flight mode. During descent the rotor wake is raised up towards the rotor disc and the proximity of the blades to the wake or even their crossing the wake region is an aerodynamic phenomena which is extremely difficult to model. The unsteady pressures generated on the rotor blades during the blade wake interaction have to be correctly predicted in order to adequately capture the BVI noise signatures. This in turn means that the wake geometry in the aerodynamics code should simulate as closely as possible the real flow situation. In order to test the capability of the code for this flight mode, a forward descent flight situation for the AH1/OLS rotor was computed. A 1/7-scale model of this rotor has been tested in the wind tunnel and the results are reported in [15]. The two blade AH1/OLS rotor has rectangular linearly twisted blades with a slightly modified NACA 0012 profile. The case chosen for the code validation exhibited severe BVI in the wind tunnel tests and has the following parameters:

$$Ma_{tip} = 0.663$$

$$\alpha_{tpp} = 1°$$

$$\Theta = 5.03° + 1.9° \cos\Psi - 2.04° \sin\Psi$$

$$\mu = 0.162$$

Here Θ denotes the blade pitch angle, Ψ the azimuth angle, μ the advance ratio and α_{tpp} the inclination of blade tip-path plane to the horizontal.

Since only a small number of pressure sensors was installed on the blade profile, a good estimation of section lift from experimental data was not possible. Instead, the 3-D Panel code prediction of the blade surface pressure is compared at one chordwise station (3%) and three spanwise (75%, 80% and 91%) stations with corresponding experimental data in Figs. 8a, b and c. The 3-D Panel code was run with an azimuth angle resolution of 5 degrees.

Even though the salient features of the pressure-time history are reproduced by the 3-D Panel code, the pressure peaks in the first and fourth quadrant shown in the experiment which are typical of the BVI, are partially - in the first quadrant with some phase shift - reproduced by the code. Improvements in the pressure correlation are expected through smaller Ψ-steps and finer discretisation of the blade profile in the leading edge area. This is a subject of future work.

Using the unsteady blade pressure data described above, the acoustic pressure-time history at several microphone locations has been computed and compared with corresponding full scale flight test and wind tunnel data from [15] in Fig. 9a. For the in-plane microphone positions 2, 6 and 8 the predicted pressure-time history does not predict the sharp positive peaks exhibited by the model scale wind tunnel results. Also the amplitude of the negative pressure pulse, except for the microphone location 6, is underpredicted.

A closer scrutiny of this discrepancy reveals that a phase shift between the predicted loading-time history and wind tunnel results may be a probable cause of the absence of the sharp (BVI) pressure peaks in the predictions. To check this, the predicted loading was shifted arbitrarily by an azimuth angle of about 14° - that is the predicted pressure occurred by this amount earlier than the experiment. Explicitly this is equivalent to shifting the theoretical predictions in Fig. 8 to the left relative to the experimental results. The thickness noise contribution remained in phase with the experiment. The sum of the so-conditioned loading and thickness acoustic pressure-time history shows an improvement in correlation with the wind tunnel experiment as shown in Fig. 9b, as an example for microphone nos. 6, 2 and 8. The reasons for this phase shift of the predicted loading are not yet clear and are the subject of further study.

Fig. 10 illustrates the agreement obtained between the predicted acoustic pressure-time history and corresponding full scale and model scale wind tunnel results for the 30° down microphone nos. 7, 3 and 9. As in Fig. 9a, the prediction results shown are without the phase shift discussed above. For these microphone positions the loading noise is known to dominate. The general features of the experimental noise signature are reproduced by the theory but the BVI spikes are not correctly simulated.

A look at Figs. 9a and 10 reveals a fairly good agreement between the predicted and full scale flight test results for the inplane and 30° down microphone positions, even though the BVI spikes are here also not properly accounted for.

The mid-frequency summary level contour plot for a plane situated 1.2 rotor diameters below the rotor hub is shown in Fig. 11. The frequencies considered are from 6th to 40th harmonics of the blade passage frequency which is equal to 75 Hertz. The sound field represented covers an area of ±4 meters up- and downstream of the hub and ±2.7 meters laterally on either side of the hub. The contour plot is based on values evaluated at 187 equidistant grid points on a 0.54 m by 0.5 m mesh in the plane considered. The numbers on the iso-lines indicate the sound pressure level in dB.

The high intensity noise radiation region for this flight condition lies ahead of the rotor slightly asymmetric to the longitudinal plane of symmetry, the asymmetry being more pronounced towards the advancing blade side. The location where the highest value of sound pressure of 105 dB occurs lies upstream on a path inclined approximately 35° downwards to the rotor disc. This result is in qualitative agreement with flight test results reported in [16].

Four Blade BO 105 Rotor in Hover and Forward Descent Flight

A further validation of the aerodynamic and acoustics code was undertaken by performing calculations for the BO 105 four blade rotor in hover and forward descent flight. A 40% scale 4 m diameter instrumented model rotor of the BO 105 has been extensively tested in the German-Dutch Wind Tunnel (DNW) in the framework of the European HELINOISE research programme. Some of the acoustics data reported in [10] is used here for the comparison with the predictions.

The wind tunnel data for the rotor in hover often includes quite a few 'contamination' effects which make a comparison with theoretical results difficult. In the DNW tests, the rotor plane was about 2.3 rotor diameters above the ground. With a nominal rotor thrust of 3600 Newton a recirculation of air in the (open) test section is to be expected which can, additionally, be asymmetrical to the tunnel plane of symmetry. A closer look at the acoustic results from [10] for the hover situation confirms this conjecture.To avoid these difficulties and enable a fair comparison with acoustic predictions for the rotor in hover, the experimental acoustics data was band pass filtered to eliminate frequencies lower than 60 Hertz and higher than 383 Hertz which correspond approximately to the 1st and 6th harmonics of the blade passage frequency value of about 64 Hertz.

The station chosen for the validation is 4 m upstream of the rotor and 2.3 m below the rotor plane. At this station, corresponding to eleven microphones placed at intervals of 0.54 m, the acoustic pressure-time history over one rotor revolution was evaluated and compared with experimental data in Figs. 12 and 13. Microphone number one is located at the laterally outmost position on the blade retreating side and microphone number eleven on the blade advancing side. The tip Mach number for the chosen hover case is 0.589 with a thrust coefficient of 0.0044.

In Fig. 12 the predicted acoustic pressure-time history (3-D Panel method calculation with 22.5° azimuth steps as input to HRNPC) is compared with the experimental results (band pass filtered experimental blade surface pressures input to HRNPC). Using the experimental blade surface pressure results as input avoids the inclusion of contaminations such as microphone self noise. In Fig. 13 the same procedure is repeated but now the actual acoustic pressure-time history measured by the microphones is used for comparison with the theoretical predictions. Even though this data is similarly band pass filtered as in Fig. 12, the agreement between theory and experiment is not so good which confirms that care has to be taken in the choice of wind tunnel data, especially for the rotor in hover, to validate the theoretical results.

As a final result of this validation study the mid-frequency summary level plots (averaged in the time domain) for the BO 105 model rotor in descent flight are illustrated in Fig. 14. The flight conditions are:

$$Ma_{tip} = 0.740$$

$$C_T = 4.484 \cdot 10^{-3}$$

$$\alpha_s = 5.05°$$

$$\Theta = 3.83° + 1.68° \cos\Psi - 1.01° \sin\Psi$$

$$\mu = 0.1495$$

with C_T as the thrust coefficient and α_s as the shaft tilt angle.

The basis of the contour plots in Fig. 14 is the acoustic pressure-time history evaluated at the grid points of a 0.54 m by 0.5 m mesh laid over a 8.0 m by 5.4 m plane lying 2.3 m below the rotor plane. The center of the plane coincides with the rotor center of rotation.

Experimental blade surface pressure was utilised as input to the HRNPC to arrive at the contour plot of Fig. 14a, whereas 3-D Panel method surface pressures served as input to the HRNPC for the contour plots of Fig. 14b. The Panel method computations were performed for azimuth steps of 5°.

Considering the high intensity noise regions from experiment and theory, the levels predicted by theory - 110 to 111 dB - match quite well with the experimental results of 111 to 112 dB. However, the location of these regions are shifted in the prediction by about 0.75 m upstream relative to the experimental results.

As discussed earlier, a number of factors, mainly in the aerodynamics code appear to be responsible for these discrepancies and need further investigation.

CONCLUSIONS

The main aim of this work was to assess the possibility of predicting the radiated sound field of a helicopter rotor in hover and forward flight purely through theoretical means. Attention was restricted to low speed shock free rotor flow and especially the descent flight where strong BVI-related noise is known to occur.

The prediction tools used are a newly developed high resolution 3-D Panel method whose aerodynamic input into an also newly developed aeroacoustics code computes the sound signature. The Panel method places no restrictions on the blade geometry and motions as well as the size of computation step. The Aeroacoustic code is based on Farassat's 1A of the FWH-equation.

The major findings of the validation study are as follows:

- In general a reasonably good prediction of the radiated sound field and its details has been obtained for two and four blade rotors in subsonic forward and descent flight.
- Very high demands are to be met by the aerodynamic data input into the aeroacoustics code. Besides very small azimuth steps, the unsteady pressure data has to simulate - time accurate - the rapid pressure changes during blade wake interaction.
- The Panel method results show a slight delay in the occurrence of BVI compared to the experiment. Precise reasons for this behaviour are not known and are the subject of further study.
- Experimental data from wind tunnel has to be carefully selected for the validation of theoretical methods, especially for the hover flight mode. It should be free of secondary effects such as flow recirculation in the test section, microphone self noise, etc.
- The sound field prediction for the UH-1H two blade rotor in hover and forward flight agrees very well with flight test results and also with computations by the well known WOPWOP acoustics code.
- Acoustic results obtained for the AH1/OLS two blade rotor in forward descent flight are in fair agreement with the flight test, wind tunnel and other code prediction results available in the literature.
- Predicted acoustic pressure-time history and mid-frequency contour plots of the radiated sound for the BO 105 four blade rotor in hover and forward descent flight are in good overall agreement with the HELINOISE wind tunnel results.

REFERENCES

[1] Schmitz, F. H.; Yu, Y. H.: "Helicopter Impulsive Noise: Theoretical and Experimental Status", NASA TM-84390, 1983.

[2] Steinhoff, J.; Ramachandran, K.: "A Vortex Embedding Method for Free Wake Analysis of Helicopter Rotor Blades in Hover", AIAA Journal, Vol. 28, p. 426, 1990.

[3] Rai, M. M.: "Navier-Stokes Simulations of Blade-Vortex Interaction Using Higher-Order Accurate Upwind Schemes", 25th AIAA Aerospace Sciences Meeting, Reno, NV, Paper No. 87-0543, 1987.

[4] Byham, G. M.; Beddoes, T. S.: "The Importance of Unsteady Aerodynamics in Rotor Calculations", AGARD Conference Proceedings No. 227 on Unsteady Aerodynamics, 1977.

[5] Giesing, J. P.: "Nonlinear Two-Dimensional Unsteady Potential Flow with Lift", Journal of Aircraft, Vol. 5, No. 2, pp. 135-143, 1968.

[6] Summa, J. M.: "Potential Flow about Three-Dimensional Streamlined Lifting Configurations with Application to Wings and Rotors", SUDAAR Rep. No. 485, Stanford University, USA, 1974.

[7] Ahmed, S. R.: "Unsteady Panel Method Calculation of Pressure Distribution on BO 105 Model Rotor Blades and Validation with DNW-Test Data", 50th Annual Forum of the American Helicopter Society, Washington D.C., 1994.

[8] Yin, J. P.; Ahmed, S. R.: "Treatment of Unsteady Rotor Aerodynamics Using a 3-D Panel Method", unpublished DLR Report, 1994.

[9] Brentner, K. S.; Farassat, F.: "Helicopter Noise Prediction: The Current Status and Future Direction", DGLR/AIAA 14th Aeroacoustics Conference, Aachen, Germany, 1992.

[10] Splettstoesser, W. R.; Niesl, G.; Cenedese, F.; Papanikas, D. G.: "Experimental Results of the European HELINOISE Aeroacoustic Rotor Test in the DNW", 19th European Rotorcraft Forum, Cernobbio, Italy, Paper B8, 1993.

[11] Lamb, H.: "Hydrodynamics", Dover Publications, New York, USA, 1932.

[12] Brentner, K. S.: "Prediction of Helicopter Rotor Discrete Frequency Noise", NASA TM-87721, 1986.

[13] Schultz, K.-J.; Splettstoesser, W. R.: "Prediction of Helicopter Rotor Impulsive Noise Using Measured Blade Pressures", 43rd Annual Forum of the American Helicopter Society, St. Louis, Missouri, 1987.

[14] Conner, D. A.; Hoad, D. R.: "Reduction of High-Speed Impulsive Noise by Blade Planform Modification of a Model Helicopter Rotor", NASA TM-84553, AVRADCOM TR 82-B-6, 1982.

[15] Splettstoesser, W. R. et al.: "Helicopter Model Rotor-Blade Vortex Interaction Impulsive Noise: Scalability and Parametric Variations", NASA TM-86007, 1984.

[16] Boxwell, D. A.; Schmitz, F. H.: "Full-Scale Measurements of Blade-Vortex Interaction Noise", J. Am. Helicopter Soc., Vol. 27, No. 4, 1982.

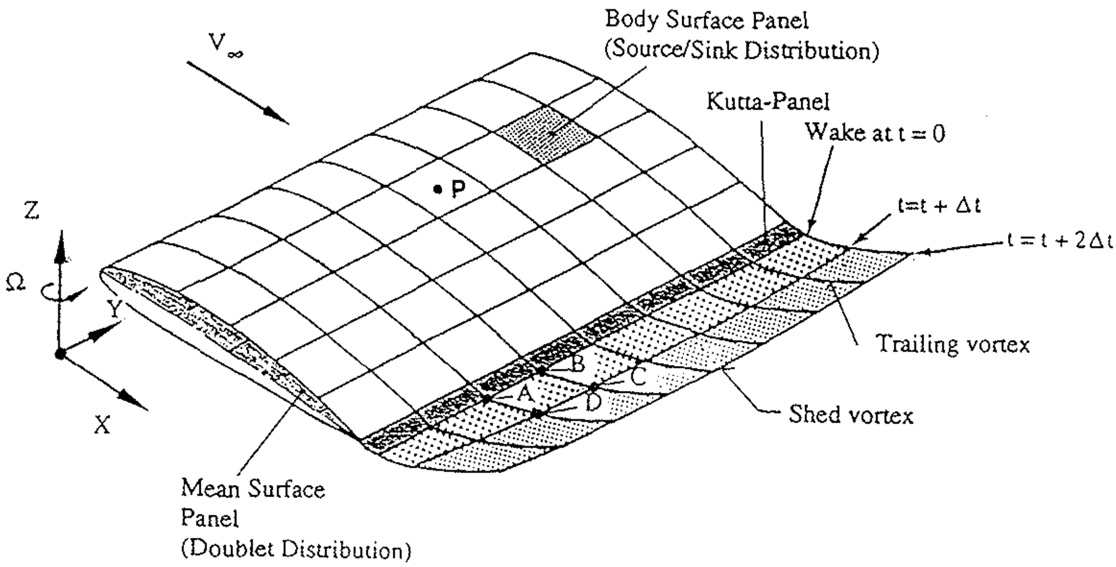

Fig. 1 Numerical Model of a Blade and Wake Segment

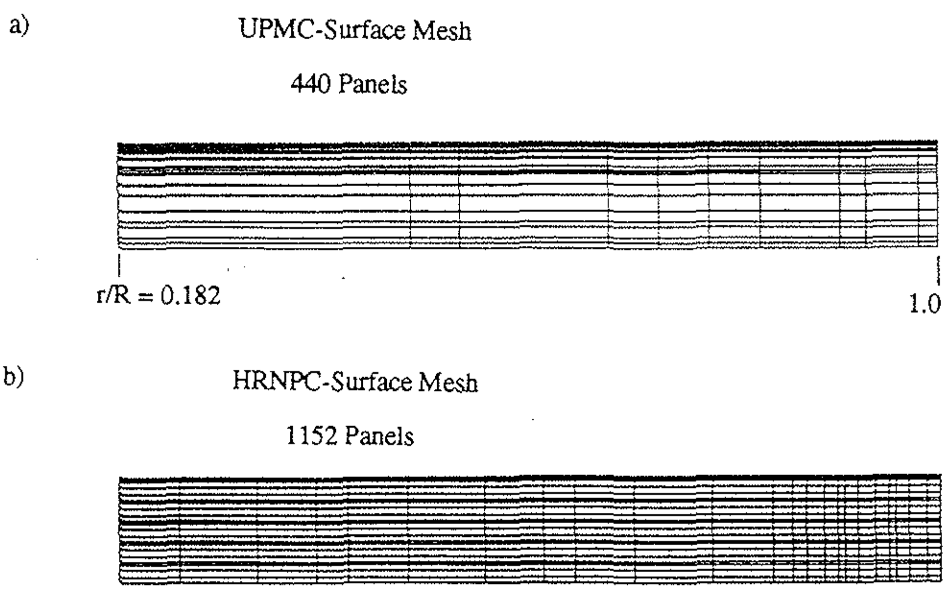

Fig. 2 Surface Discretisation of one blade of the AH1/OLS Rotor for
a) 3-D Panel Method, and
b) Acoustics Code

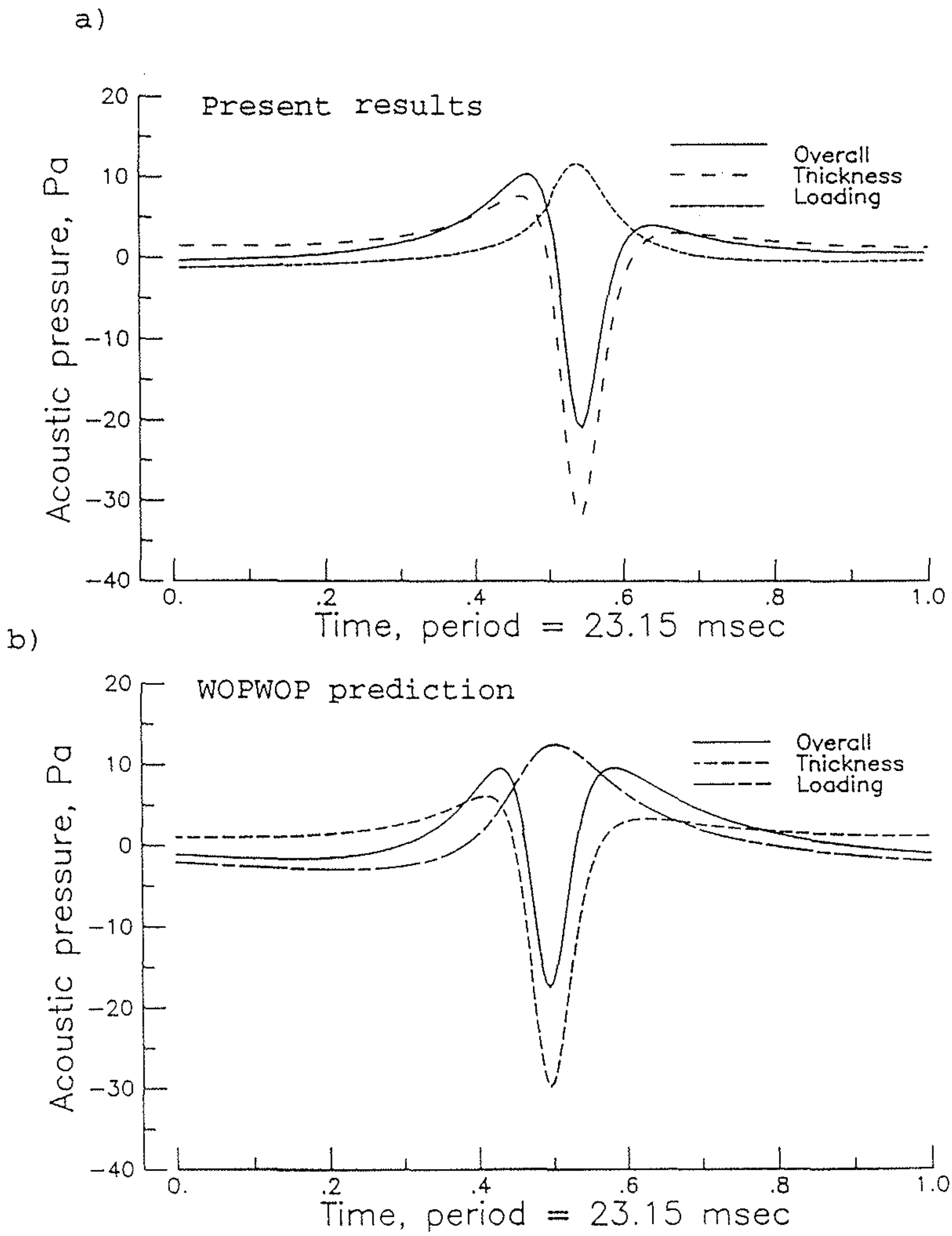

Fig. 3 Acoustic pressure-time history for the 2-blade UH-1H rotor in hover
a) Present results and b) WOPWOP predictions

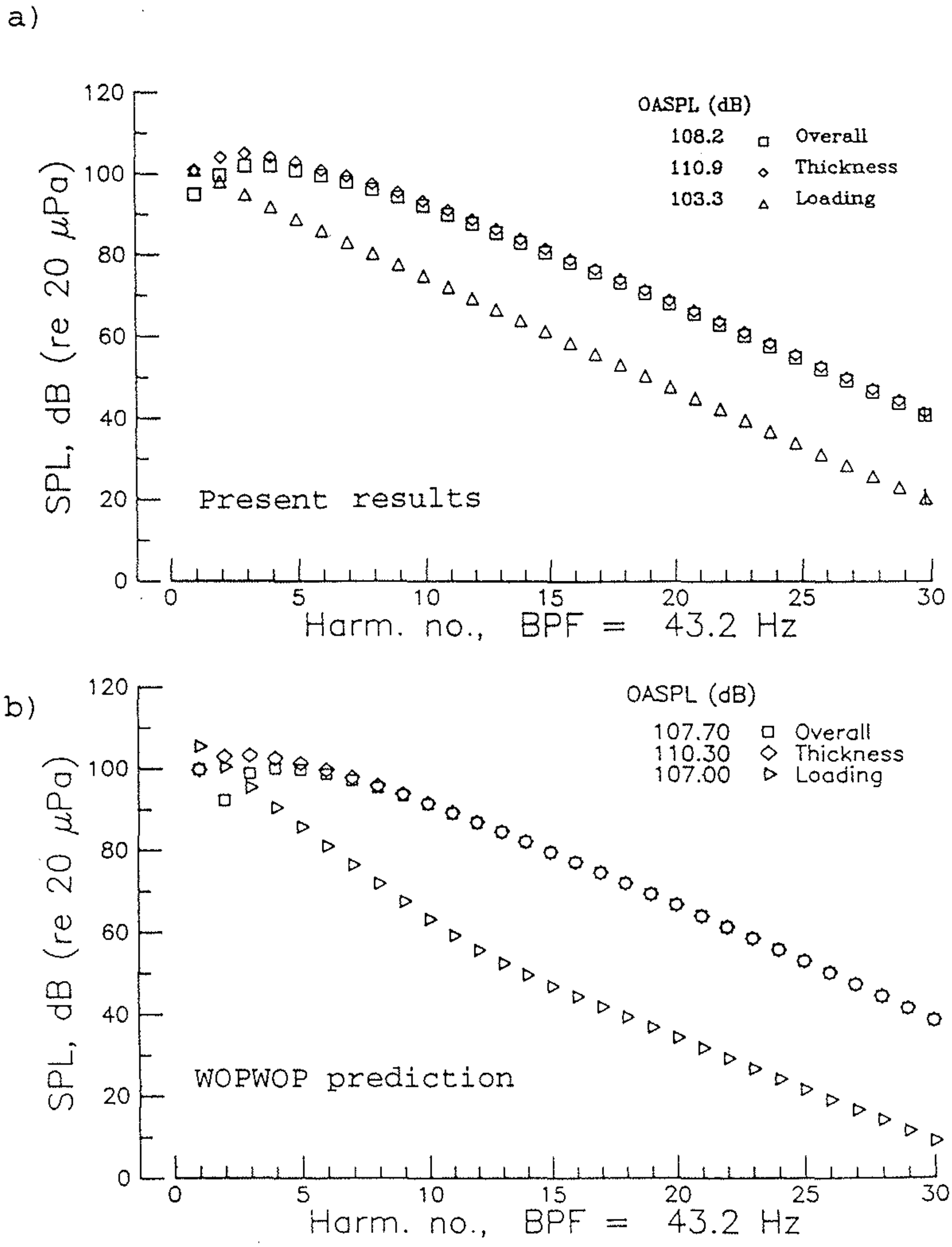

Fig. 4 Sound pressure level for the 2-blade UH-1H rotor in hover
a) Present results and b) WOPWOP predictions

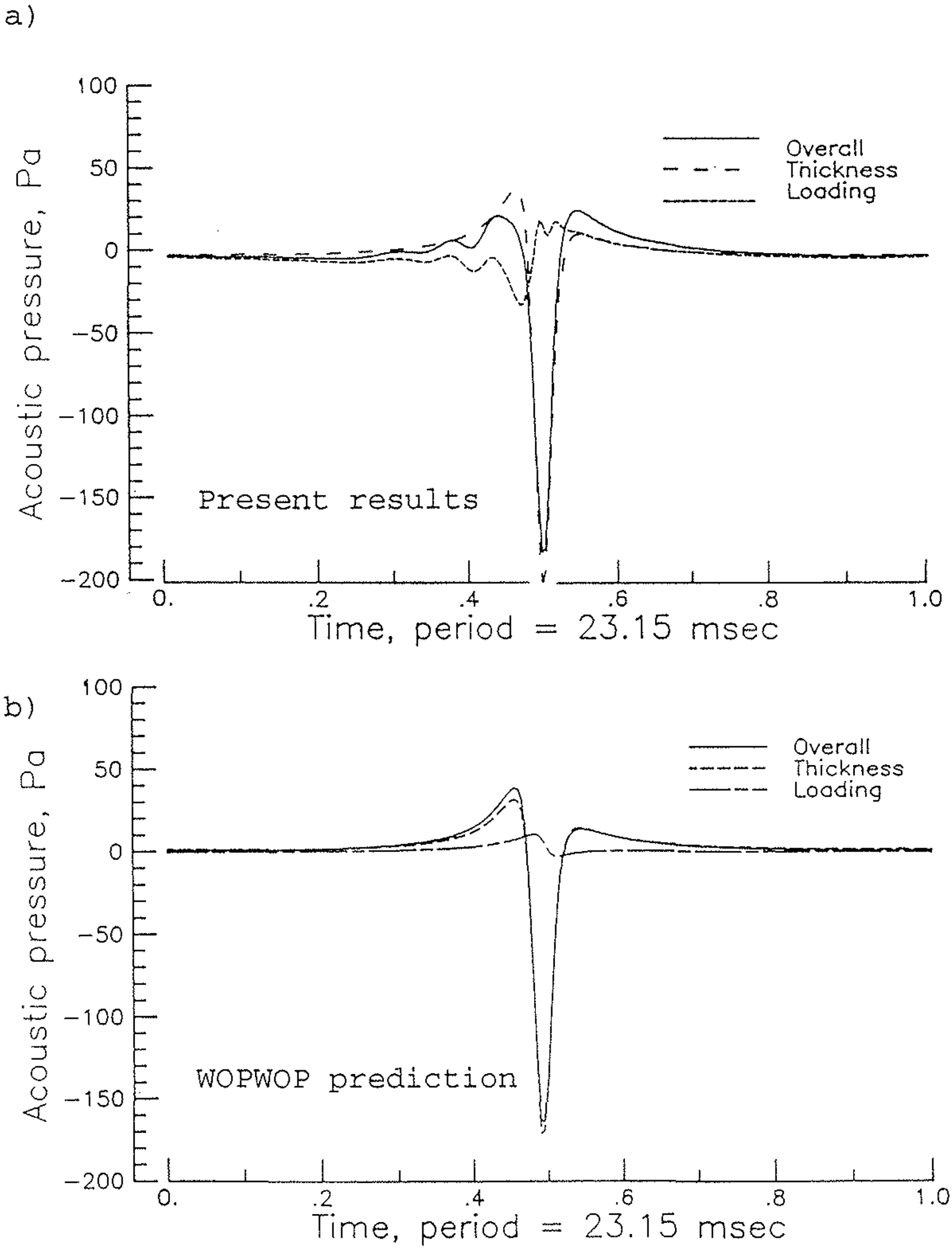

Fig. 5 Acoustic pressure-time history for the 2-blade UH-1H rotor in forward flight
a) Present results b) WOPWOP predictions

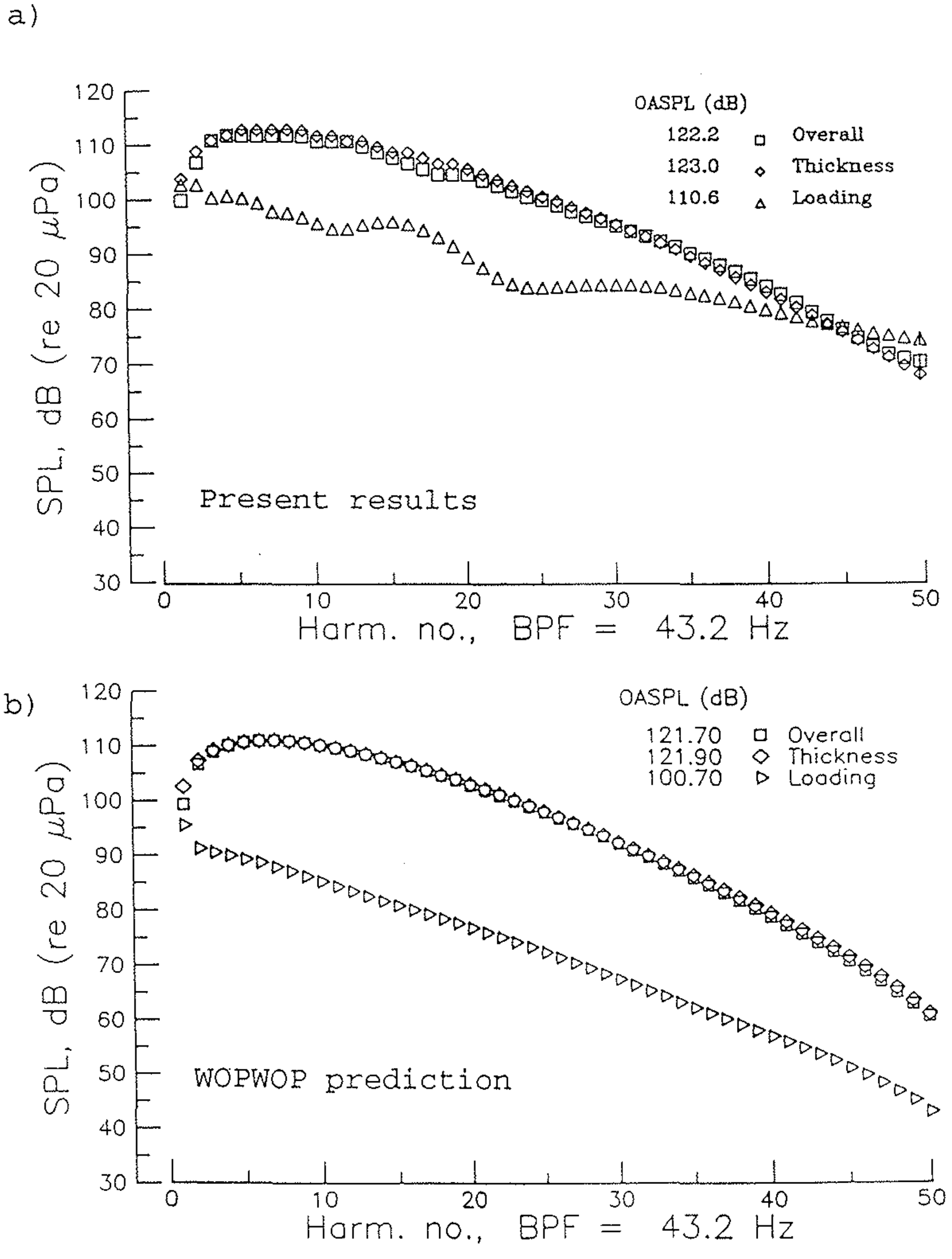

Fig. 6 Sound pressure level for the 2-blade UH-1H rotor in forward flight
a) Present results b) WOPWOP predictions

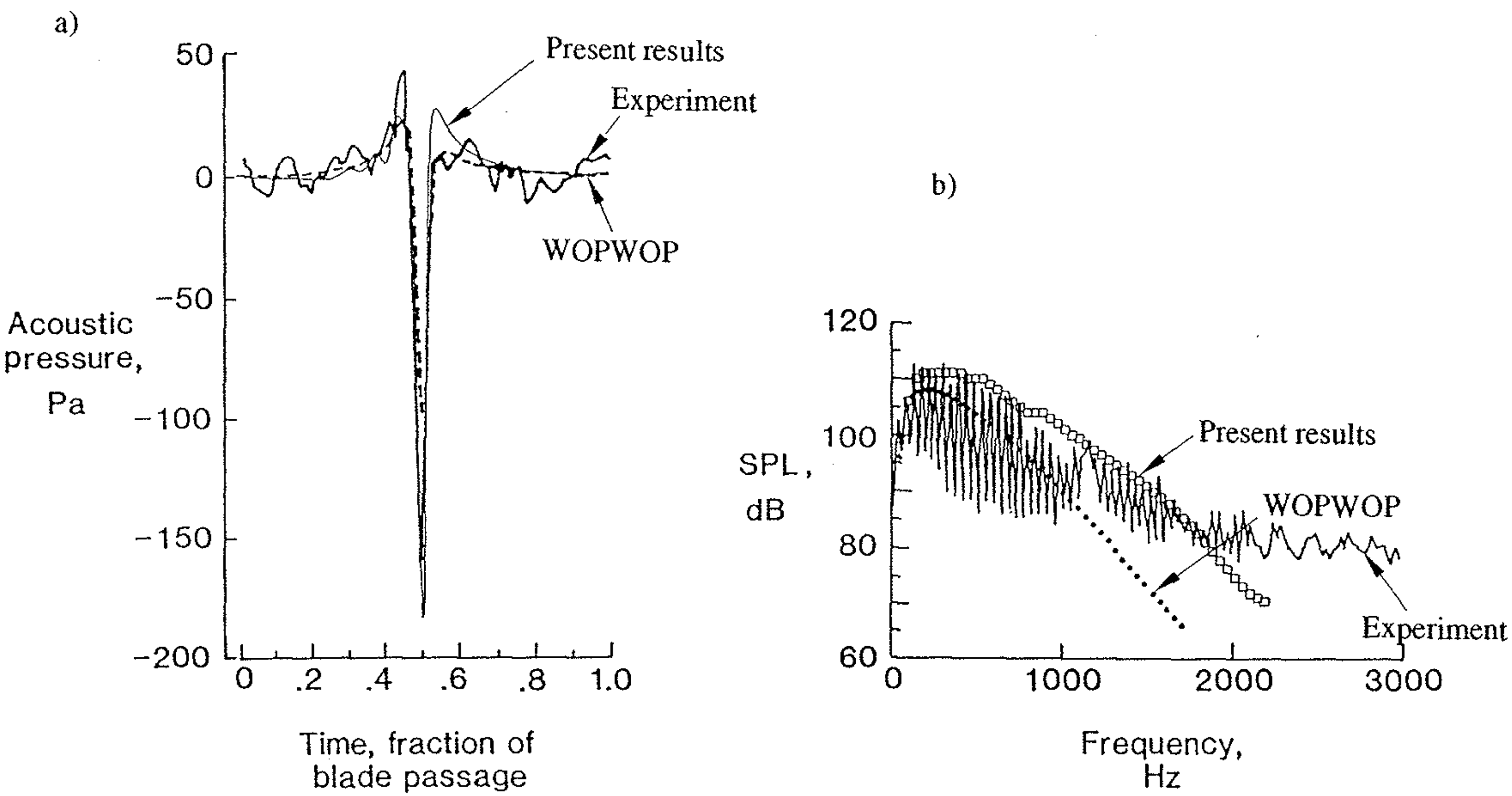

Fig. 7 Two-blade UH1-UH rotor in forward flight
a) Acoustic pressure-time history, and b) Sound pressure level, comparison of present results with WOPWOP predictions [12] and model scale experiments [14]

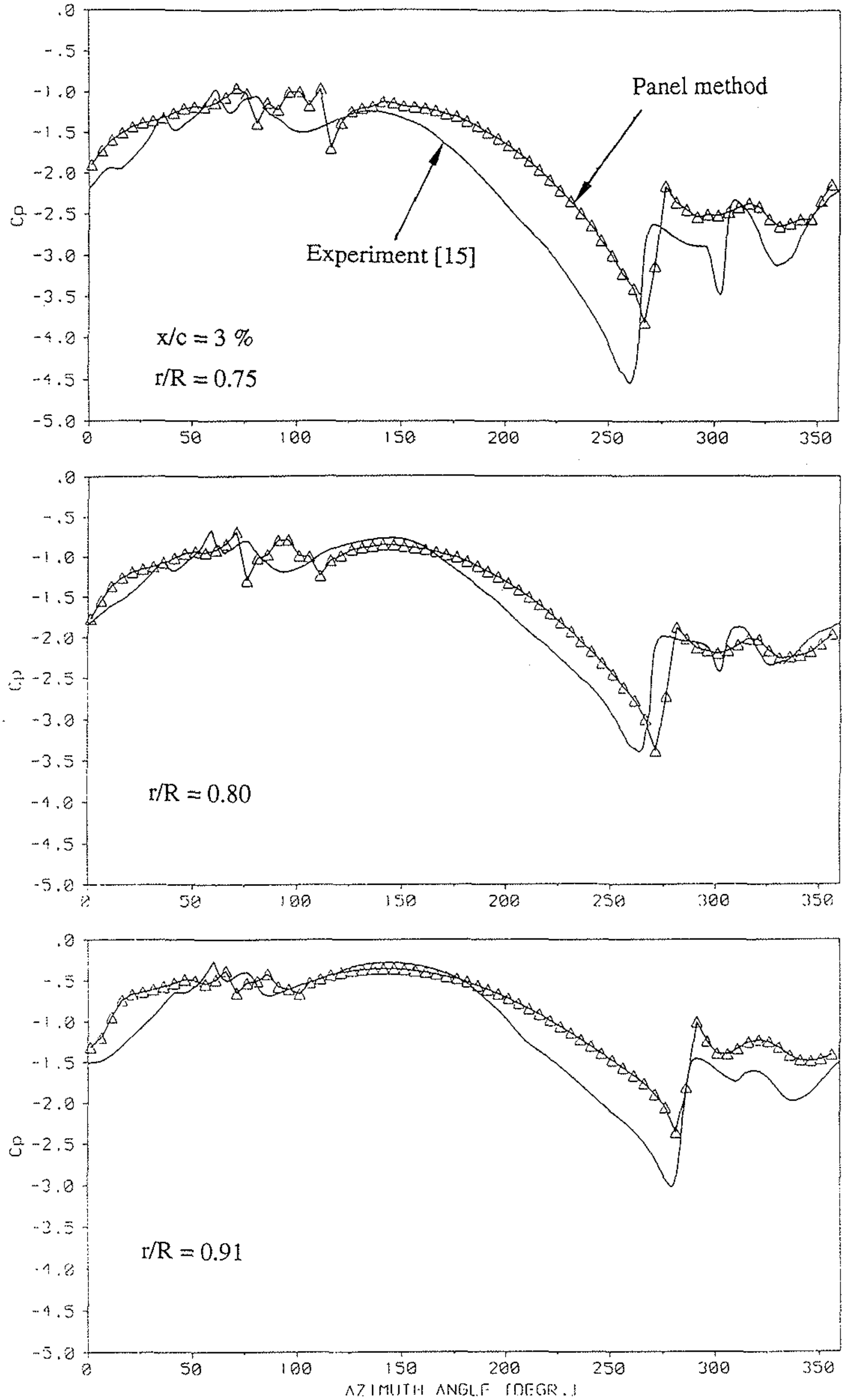

Fig. 8 Pressure-azimuth angle history at 3 % chord and at 75 %, 80 % and 91 % blade span stations Two-blade AH1/OLS rotor in forward descent flight. Comparison of Panel method prediction and experiment

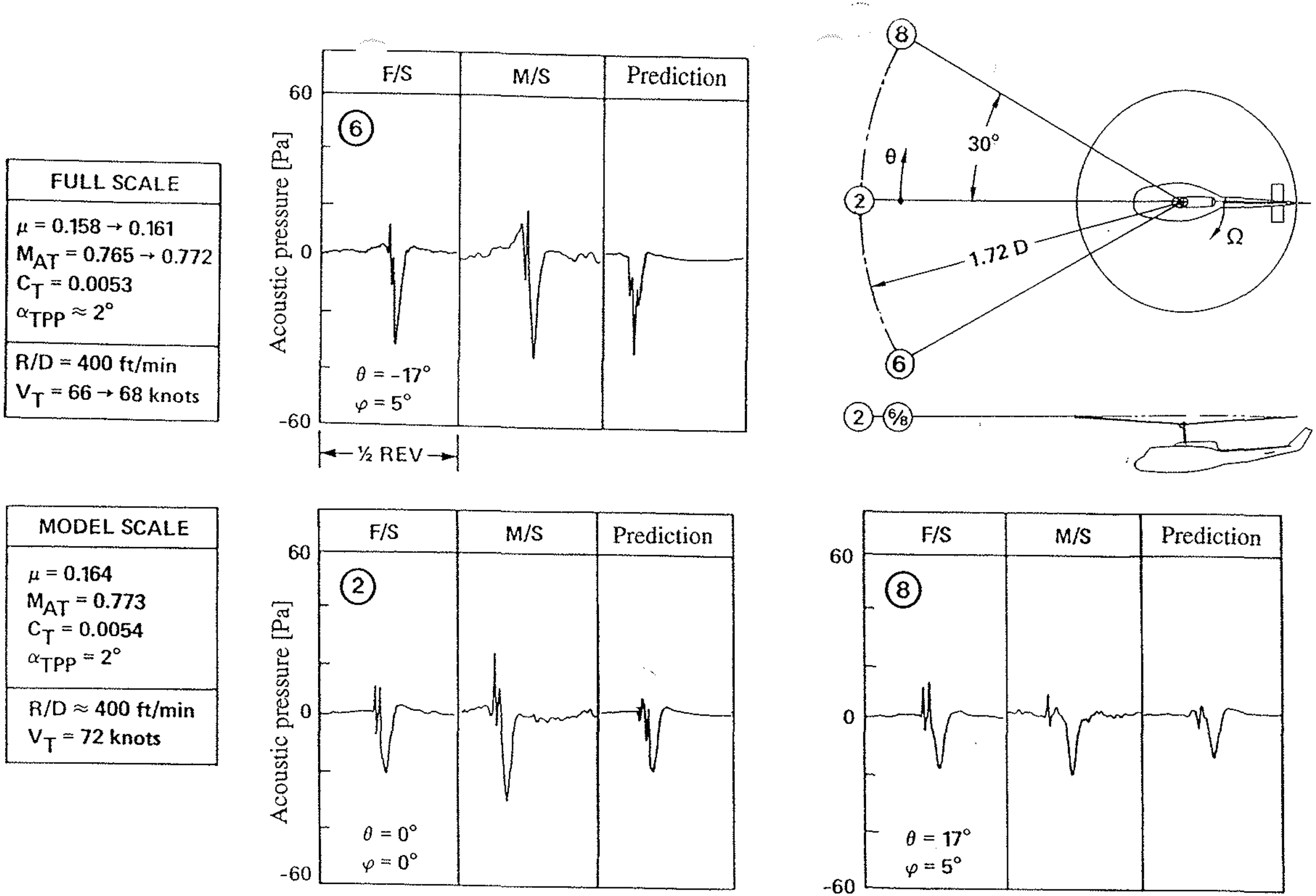

Fig. 9a Acoustic pressure-time history for in-plane microphone positions. AH1/OLS rotor in descent flight. Comparison of prediction with flight test (F/S) and wind tunnel (M/S) results.

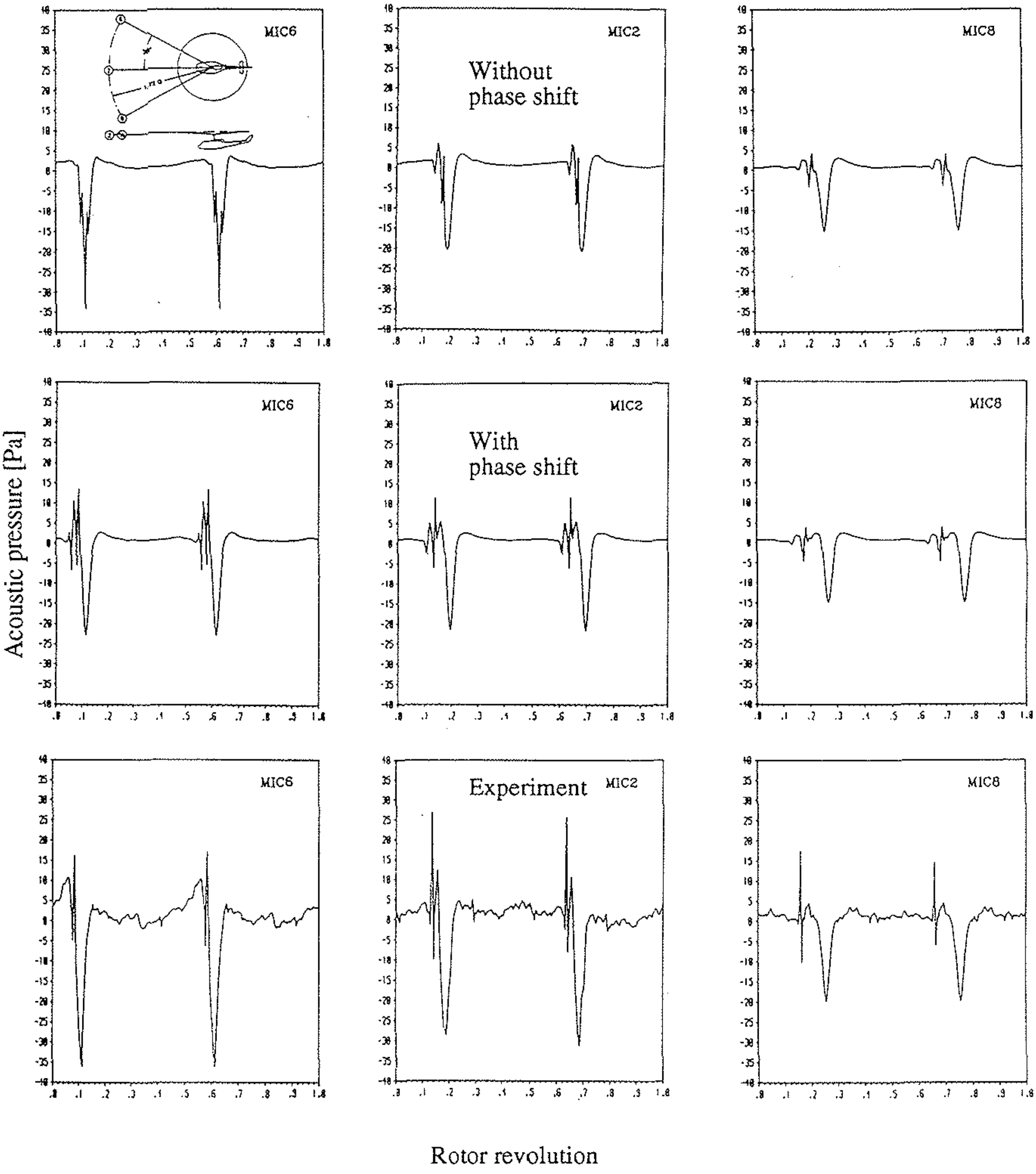

Fig. 9b Effect of a phase shift of predicted loading time history on the overall acoustic-pressure history. AH1/OLS rotor in forward descent flight.

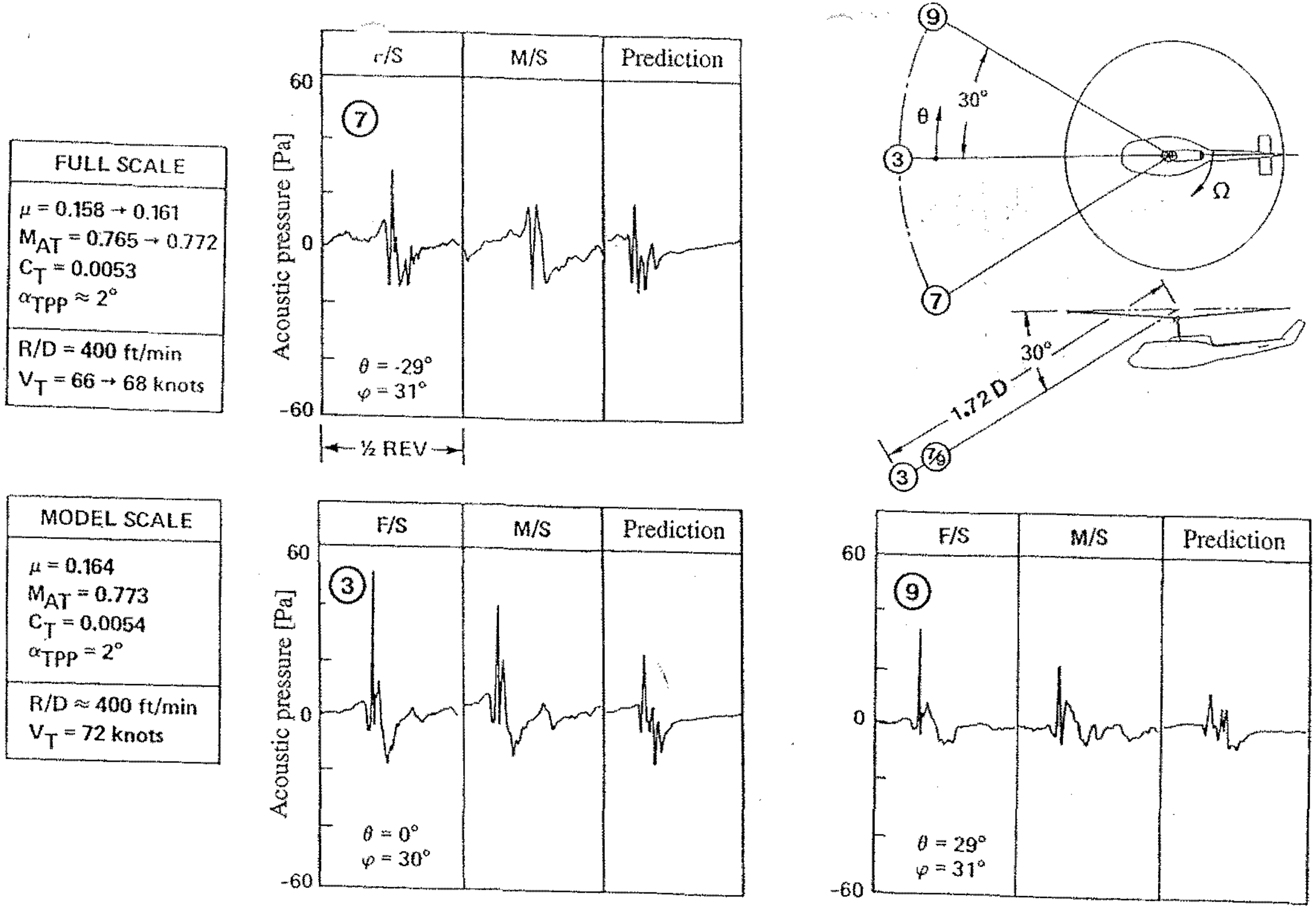

Fig. 10 Acoustic pressure-time history for 30° down microphone positions. AH1/OLS rotor in descent flight. Comparison of prediction with flight test (F/S) and wind tunnel (M/S) results.

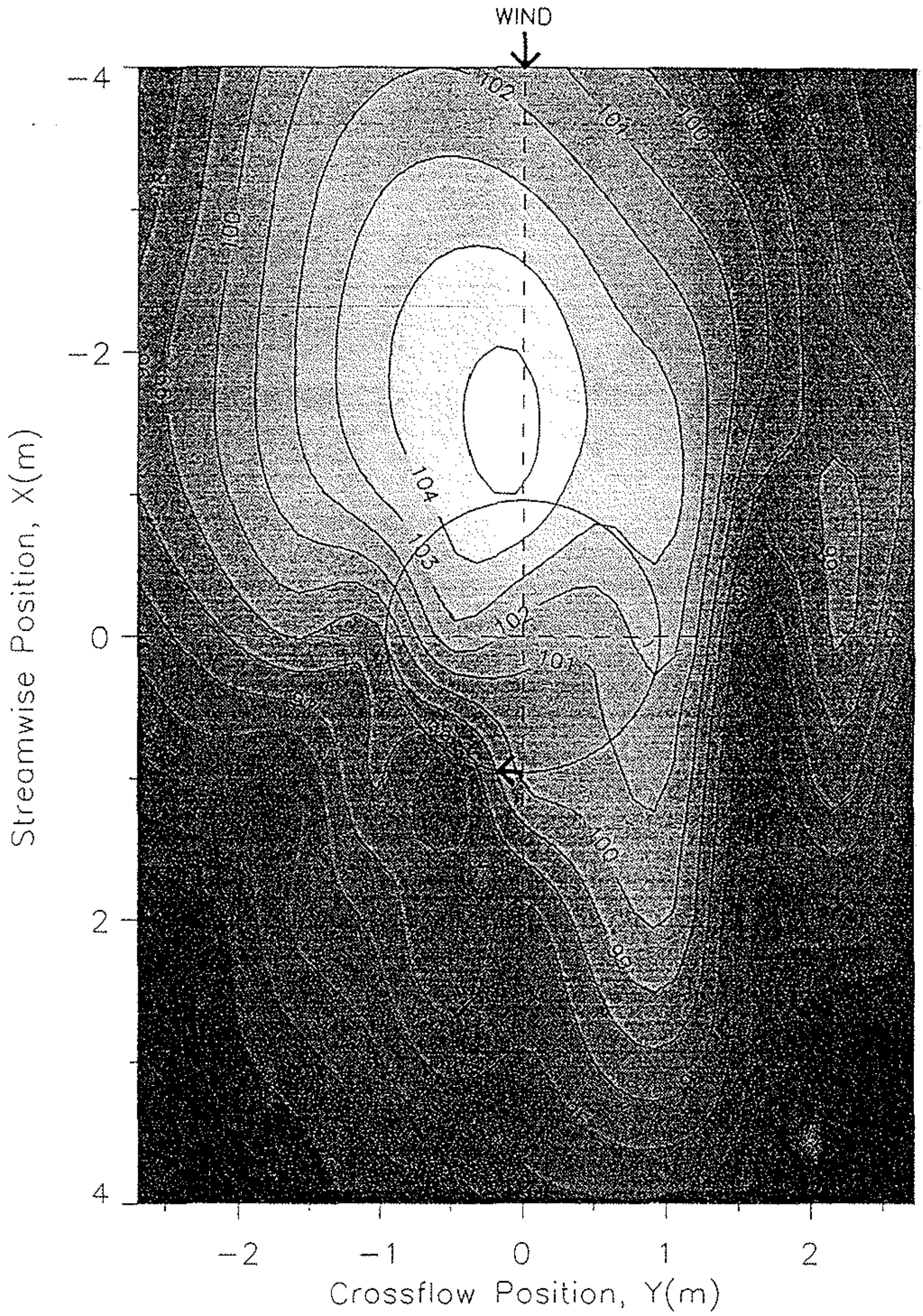

Fig. 11 Mid-frequency level contour plot for a plane 1.2 rotor diamters below the rotor. AH1/OLS rotor in descent flight. $Ma_{tip} = 0.663$; $\mu = 0.162$; $\alpha_{TPP} = 1°$

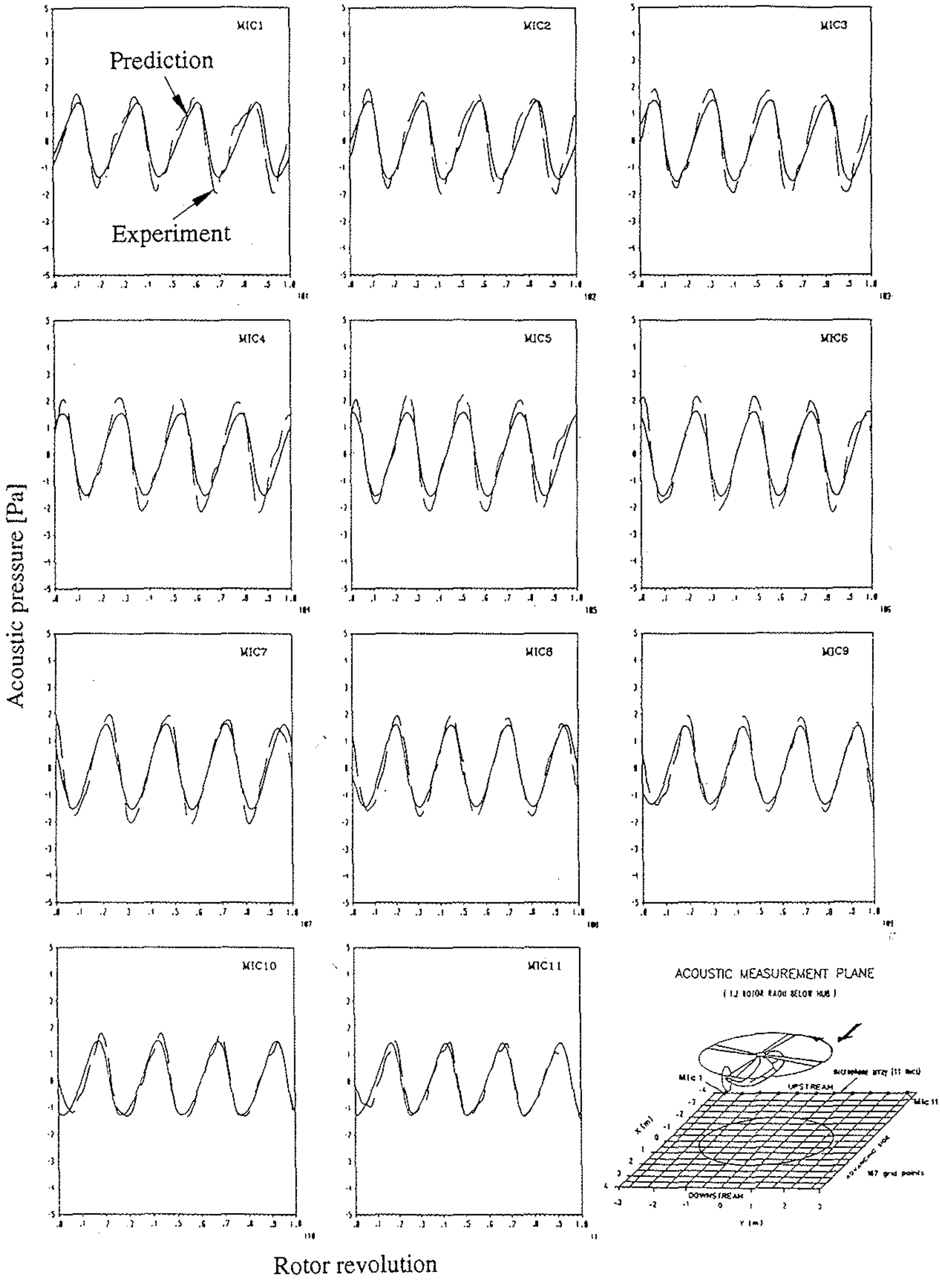

Fig. 12 Acoustic pressure-time history 4 m upstream of rotor hub and 2.3 m below the rotor plane. Experimental result obtained with *measured blade surface pressure* (band pass filtered) as input to HRNPC. BO 105 four-blade rotor in hover. $Ma_{tip} = 0.589$; $C_T = 0.004$

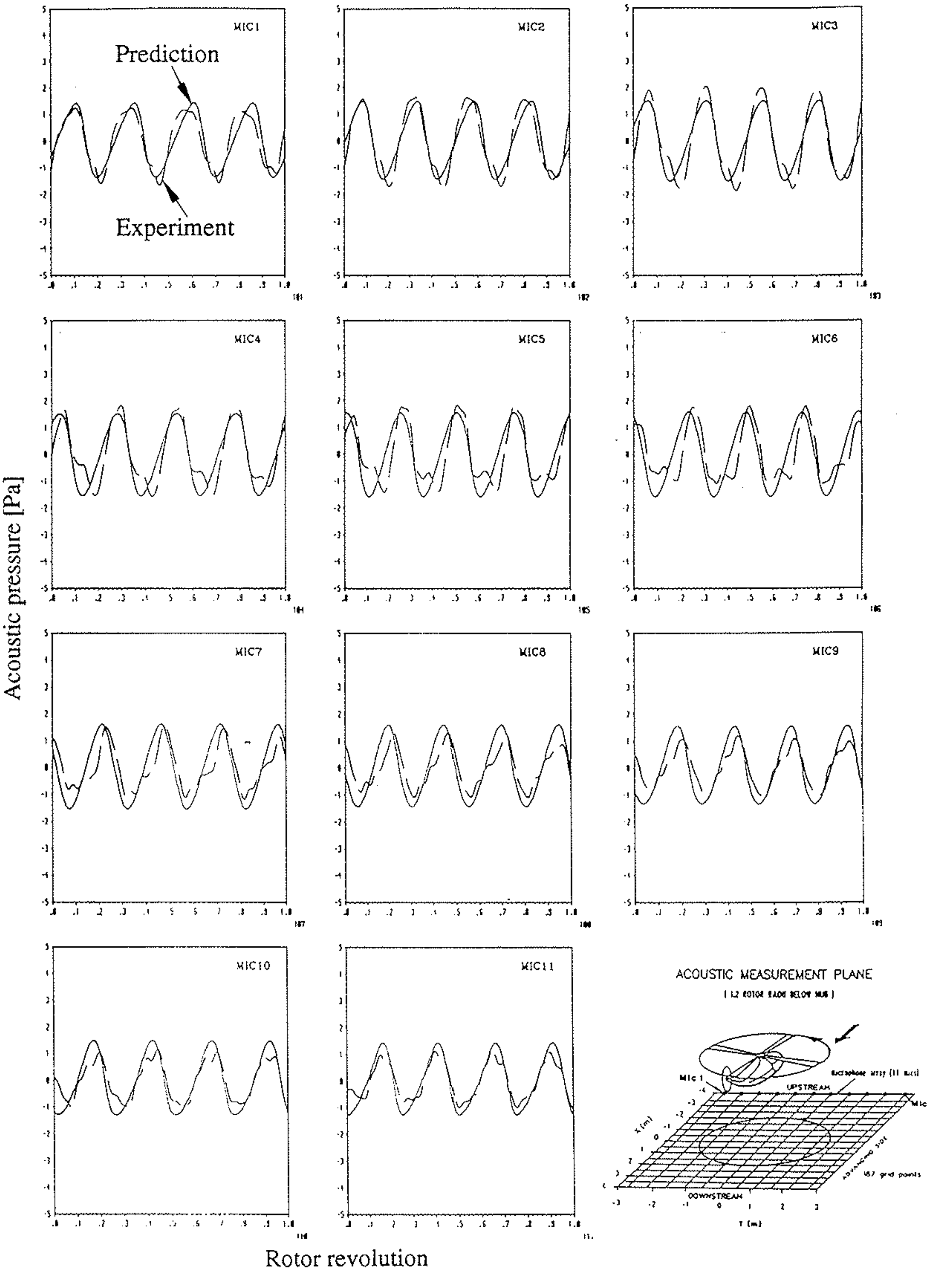

Fig. 13 Acoustic pressure-time history 4 m upstream of rotor hub and 2.3 m below the rotor plane. Experimental data is *microphone measurements* (band pass filtered). BO 105 four-blade rotor in hover. $Ma_{tip} = 0.589$; $C_T = 0.004$

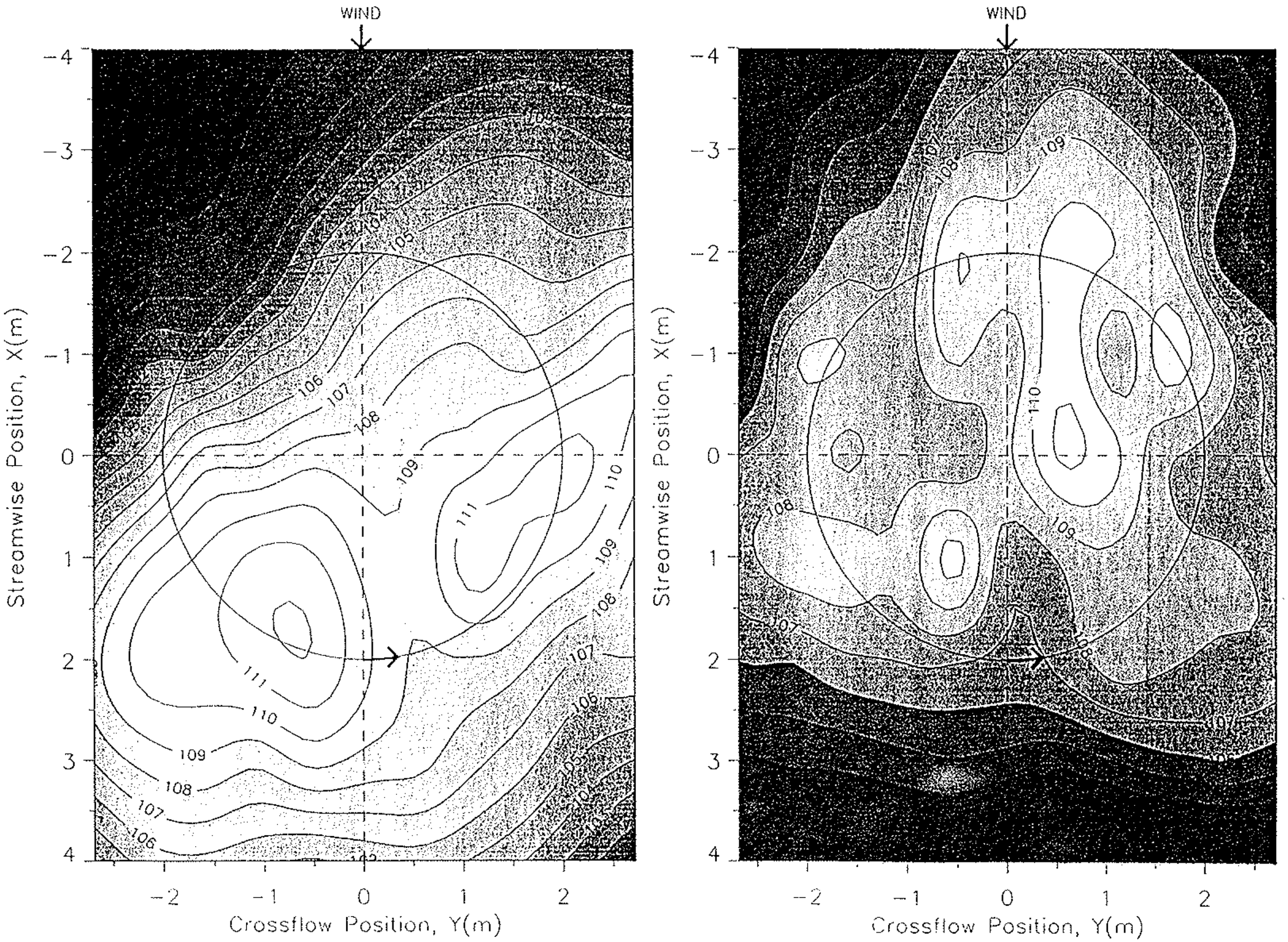

Fig. 14 Mid-frequency level contour plot for a 5.4 m x 8 m plane 2.3 m below rotor plane.
a) *Experimental* blade surface pressure as input to HRNPC; b) *Panel method* blade surface pressure as input to HRNPC.
BO 105 four-blade rotor in forward descent flight. $Ma_{tip} = 0.74$; $C_T = 0.0045$; $\mu = 0.15$; $\alpha_s = 5.05°$